

A game-changing equation during the etching of tuning forks and its verification through experiments

Kadir Can Erbaş^{*}, Mebrure Erdoğan, Dilek Çökeliiler Serdaroğlu, İsmail Cengiz Koçum

Department of Biomedical Engineering, Baskent University, Bağlıca, Turkey

ARTICLE INFO

Keywords:

Sensors
Tuning forks
Mass measurement
Frequency measurement

ABSTRACT

Quartz tuning fork (QTF) sensors, characterized by simplicity, low cost, and high-quality factor, represent a significant subset. This study delves into the etching dynamics of QTF systems, crucial for sensor applications like quartz crystal microbalance (QCM). Both theoretical and experimental investigations into QTF etching, via methods like electro-etching for large-scale tuning forks (TF) and low-pressure radio frequency (RF) plasma treatment for QTFs, have been conducted. Surprisingly, post-etching measurements reveal a lower vibrational frequency for both large-scale TFs and QTFs compared to their bare counterparts, unlike QCM sensors. A novel formula correlating this frequency reduction to mass loss has been proposed and validated through lots of experiments. Notably, longitudinal homogeneity emerges as a pivotal factor influencing the accuracy of the proposed formula. In summary, the novel mathematical framework presented herein is poised to catalyze the widespread adoption of low-cost QTFs as mass-sensitive biosensors, marking a significant advancement in the field.

1. Introduction

Molecule-specific sensors rely on a functionalized sensing layer that can detect target molecules, and this layer is of great importance for sensor performance [1]. By etching, specific surface morphologies can be obtained and desired sensing mechanisms can be created on sensor surfaces. Etching is a frequently used method in sensor systems, both to ensure the sensitive detection of some analytes, to enhance the sensing mechanism, and in sensor design and sensor production processes [2,3,4,5,6,7,8,9,10,11]. In biosensors, the natural or designed surface topography has profound effects on the events occurring at the bio-interface, such as the immobilization and activity of biomolecules. For example, surface roughness is an important factor in bio-immobilization efficiency and the target analyte binding capacity of the bio-interface [12]. This surface roughness can also be obtained by etching processes. On the other hand, etching can be used as an intermediate step in biosensor configurations. One reason for this is that biological molecules may have an adsorption enhancing effect and this has been shown to increase the sensitivity [13]. The use of etching in molecularly imprinted polymers based mass sensitive sensors, frequency regulation by etching is also possible [14,15]. In addition, etching steps can be applied before forming layers on the mass sensitive sensor [16]. It is therefore

important to study the etching mechanism in mass sensitive sensors. Studies have also been reported in the literature that the etching of nanoparticles grown on the surface of biosensors has been used to develop plasmonic nanosensors by modulating the size and morphology of nanoparticles for biosensing applications [17], to clean the sensor surface [1,16] and to increase biosensing sensitivity [18].

Presently, piezoelectric quartz resonators are mechanical transducers used for chemical and biological sensor devices that convert the mass or thickness of a foreign layer of an analyte to an electrical signal. In quartz crystals, the linear relationship between the frequency response and the mass accumulated on the crystal surface was discovered by Sauerbrey in 1959. After this discovery, quartz resonators have gained importance and are used as signal generators or reference systems in all kinds of electronic devices such as watches and computers, thanks to their extraordinary properties [19]. Among various piezoelectric resonators Quartz tuning forks (QTFs), which are bending based mass-sensitive sensors, have high sensitivity due to their high-quality factor. Therefore, they have become a widely used component in frequency measurement due to their features such as high frequency stability, sharp frequency response, repeatability in measurements, low cost, and low power consumption [20,21]. QTFs are used in many different fields such as light-induced thermoelastic spectroscopy (LITES)

^{*} Corresponding author.

E-mail addresses: kcerbas@gmail.com, kcerbas@baskent.edu.tr (K.C. Erbaş).

technology to improve sensitivity [22,23,24,25,26], velocity and acceleration measurements [27,28], humidity sensor [29], viscosity measurement of liquids [30], measurements of force, pressure and temperature parameters [31,32,33], density measurement of liquids [34,35], atomic force microscope [36,37], gas sensor [38,39,40] and quartz-enhanced photoacoustic spectroscopy (QEPAS)-based sensor applications [41,42,43,44] and recently biosensor studies [27,45,46,47]. With the QTF sensor system, picogram level mass change can be detected [48]. With these extraordinary properties, QTF is an alternative to the quartz crystal microbalance (QCM), which is the most popular shear-based mass sensor known for measuring small changes in mass, which is very stable and sensitive, based on the relationship between changes in the mass of the material attached to the crystal and the oscillation frequency of the crystal [19].

In QCM applications, which are alternatives to QTF, etching studies are used for frequency adjustment in the resonator production process [15], to ensure that the QCM regains its sensitivity [49], to clean the surface in biosensor applications [1,16] and to design the quartz crystal for high-precision measurements for biosensing [14]. In addition, it has been reported that the sensitivity of QCM sensors is related to the increase in the resonance frequency, and therefore chemically milled QCM biosensor studies have been reported to increase biological detection [50,51].

As mentioned above, in QCM sensors, which are the most widely used mass-sensitive sensors, the resonance frequencies of the sensor increase due to the decreasing mass from the crystal surface as a result of etching the sensor electrodes or the quartz surface in the bare state [15,52,53] and etching the material coated on the sensor surface [54,55,56]. However, in QTF, which is also a mass-sensitive sensor like QCM, it has been observed that the QTF sensor frequency decreases because of etching the bare sensor surface with etching, unlike QCM. Studies in the field of QTF have just begun, and studies in the field of etching are generally seen in the production stage of these sensors [10,11] and there is only one study in the literature reports that the frequency of the sensor decreases when the sensor surface is etched. The focus of this study, in which the metal electrodes on the QTF surface were etched, is to increase the permeability of laser adsorption of the sensor system, and the decrease in the sensor frequency with etching of the QTF sensor surface has not been studied in detail [39]. The geometric structure of QTF is more complex than QCM, and in contrast to QCM, frequency decreases can occur with etching of QTF in the bare state.

The purpose of this study is to reveal the mathematical and experimental investigation of the studies on etching of the QTF system, which is an alternative to the most widely used QCM mass-sensitive sensors and which will be used in its applications in the future. For this reason, the QTF sensors in the bare state were etched by low-pressure radio frequency (RF) plasma and the large-scale tuning fork (TF) surfaces were electrochemically etched. The experimental and theoretical frequency shifts comparisons were made. It has been experimentally and theoretically proven that the frequency of TFs decreases when they are homogeneously etched from the bare state. Since the electrode design affects the homogeneity of the etching in the electro-etching case, etchings were performed by trying different electrode designs. In addition, a new mathematical concept (fractional mass sensitivity) dependent on the homogeneity of the etching was proposed and the correctness of this concept was proved by experimental studies.

2. Theoretical background and our thesis

2.1. Calculation of frequencies of bare TF, QTF and QCM

Tuning Fork is an acoustic resonator composed of elastic metal rods with U-shaped, fork structure. They emit sound waves at a single frequency when hit on a surface or object. A tuning fork can be modeled as a damped oscillating cantilever beam. Therefore, the frequency formula

of TF can be obtained from the oscillation calculations of the cantilever beam [34,57]. While tuning forks are made of various metal materials, quartz tuning forks consist of two quartz beams with applied electrodes [58]. Quartz is a crystal exhibiting piezoelectric effect and these crystals start to vibrate when they are excited by a signal close to the natural vibration frequency [59]. TF resonance frequencies are determined by the elastic properties of the constituent material (Young's modulus) and their shape and dimensions [60]. The dimensions of the TF with circular cross-section and the QTF with rectangular cross-section are shown schematically in Fig. 1 and their dimensions are compared with a real photograph in Fig. 2. In Fig. 1.a, r represents the cross-sectional radius of the TF with a circular cross-section. In Fig. 1.b, a and b represent the cross-section lengths perpendicular and parallel to the vibration direction, respectively. L , defined as the effective length, is the distance between the zero-vibration point and the tip of the TF.

The prongs of tuning forks vibrate in a symmetric mode corresponding to the first fundamental mode of a cantilever beam [57]. In this study, the frequency of the tuning fork is modeled according to the first fundamental mode of a fixed-end beam oscillation. The Euler-Bernoulli beam theory explains the oscillation of a beam as follows:

$$-EI \frac{\partial^4 y}{\partial x^4} = \mu \frac{\partial^2 y}{\partial t^2} \quad (1)$$

where E , I , and μ represent the Young's modulus, second moment of area of the cross-section, and linear mass density of the beam respectively [61]. In this equation, x is the distance of a point on the beam from the fixed support, y is the deviation from equilibrium and t is time. The solution of this partial differential equation (PDE) gives the angular frequency formula for the first mode, as shown in Equation (2) [42,62,63].

$$\omega = \frac{3.516}{L^2} \sqrt{\frac{EI}{\mu}} \quad (2)$$

The term EI is called the *flexural rigidity*, which gives the resistance offered by a structure during bending, and L is the effective length of the beam [64]. Since the second moment of area (I) and the linear mass density (μ) vary depending on the cross-section of the beam, these values can be written for TFs with circular and rectangular cross-sections as follows:

$$I_{\text{circ}} = \frac{\pi}{4} r^4 \quad (3)$$

$$\mu_{\text{circ}} = \rho \pi r^2 \quad (4)$$

$$I_{\text{rect}} = \frac{1}{12} ab^3 \quad (5)$$

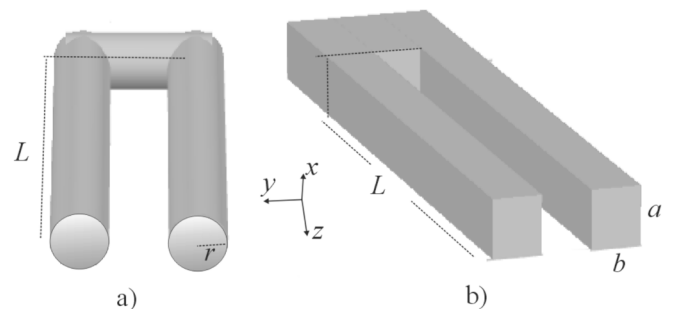


Fig. 1. Schematic representation of the dimensions and the coordinate system used. **a)** Large-scale tuning fork with a circular cross-section with $r = 1.5$ mm and $L = 7.2$ cm. **b)** Quartz tuning fork (QTF) with a rectangular cross-section with $a = 0.27$ mm $b = 0.54$ mm and $L = 6$ mm. The direction of vibration is on the y -axis and the fork length is on the z -axis.

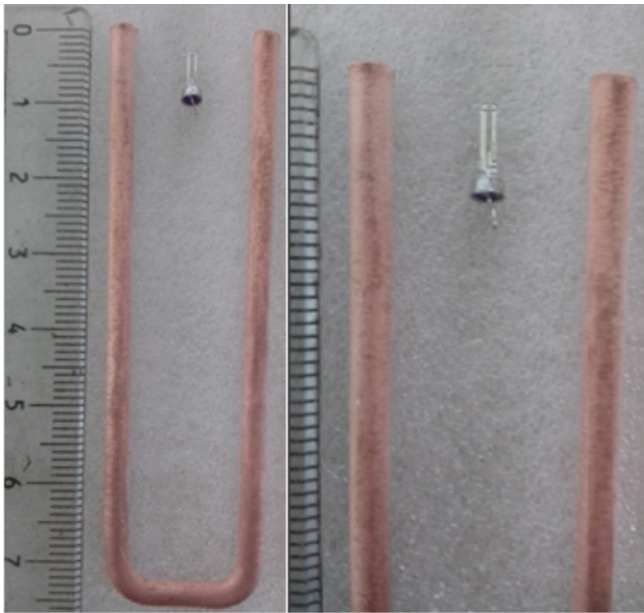


Fig. 2. Dimensional comparison of large-scale tuning fork and quartz tuning fork.

$$\mu_{\text{rect}} = \rho ab \quad (6)$$

where r is the radius of the TF with circular cross-sectional area, ρ is density. The Young's modulus of the large-scale copper TFs used for etching in this study is 130 GPa [65] and the density is 8.96 g/cm^3 , while the Young's modulus of quartz for QTFs is $7.87 \times 10^{10} \text{ N m}^{-2}$ and the density is 2600 kg m^{-3} [66]. By substituting I and μ in Equation (2), the resonant frequency formulas for circular and rectangular TFs can be rewritten as follows:

$$f_{\text{circ}} \cong \frac{0.28}{L^2} r \sqrt{\frac{E}{\rho}} \quad (7)$$

$$f_{\text{rect}} \cong \frac{0.161}{L^2} b \sqrt{\frac{E}{\rho}} \quad (8)$$

For QCM sensors, the resonance frequency formula:

$$f_Q \cong \frac{1}{2h_Q} \sqrt{\frac{G}{\rho_Q}} \quad (9)$$

where h_Q is the thickness of the resonator, G and ρ_Q are the shear modulus ($2.947 \times 10^{11} \text{ g cm}^{-1} \text{ s}^{-2}$) and the density (2.648 g cm^{-3}) of the quartz resonator respectively [67].

According to Equation 7, the values of E and ρ remain constant during the etching of a TF with a circular cross-section, while the values of radius r and length L decrease. However, if etching causes an equal decrease in all dimensions, the decrease in the value of r will be more dominant than the decrease in the value of L . According to Equation 8, which explains the frequency of a TF with a rectangular cross-section, the values of E and ρ again remain constant. If etching causes an equal decrease in all dimensions, the proportional decrease in the parallel cross-section length b will be more dominant than the proportional decrease in length L . For these reasons, the frequencies of TFs will decrease with homogeneous etching.

According to equation 9, where the resonance frequency formula of QCM is explained, while G and ρ_Q values remain constant during etching, the h_Q value, that is, the thickness of the resonator, will decrease. It is clearly seen from here that in case of etching, the fre-

quency of the QCM will increase as its thickness decreases.

The equations mentioned above for the etching condition are assumed to be valid under the following assumptions:

Assumption 1: Throughout the TF, etching is carried out uniformly.

Assumption 2: The uniformity of the cross-section scale has a significant impact on the frequency of the beam. Therefore, under the same mass, whether the mass distribution in the length direction is uniform directly affects its natural frequency, so the scale measurement after etching is crucial. The cross-section of TF is circular, and the etching takes place only on the side surfaces of the TF. This means that the radius shrinks uniformly, while the length does not change. If the reduction in radius during etching is considered to be proportional to the lateral surface area of the cylindrical fork and the reduction in length is considered to be proportional to the cross-sectional area, it can be predicted that the reduction in length will be relatively negligible. In the experiments, it was observed that the radius of the over-etched TF was almost halved, but there was no observable change in its length.

Assumption 3: During electrochemical etching, the effect of anode mud or some impurities deposited on the surface is neglected.

Under these assumptions, frequency shifts of large-scale TFs with circular cross-sectional areas in the etching condition were experimentally measured and calculated.

Fractional mass sensitivity of tuning fork: A new approach.

Using the mass, density and volume relationship, the radius of a TF of circular cross-section is calculated as follows:

$$r = \sqrt{\frac{m_T}{\pi \rho L_T}} \quad (10)$$

where m_T is the total mass of the TF, ρ is the density of the layer, r is the radius of the TF, and L_T is the total length of the TF. Substituting the value of r in Equation (10) in Equation 7 gives

$$f = \left(\frac{0.28}{\rho L^2} \sqrt{\frac{E}{\pi L_T}} \right) m_T^{1/2}. \quad (11)$$

In Equation (11), taking the logarithm of both sides results in Equation (12), and then taking the derivative of Equation (12) results in Equation (13). Since it is assumed that L (effective length) and L_T (total length) will not change with etching, these values are taken as constant when taking the derivative.

$$\ln f = \ln \left(\frac{0.28}{\rho L^2} \sqrt{\frac{E}{\pi L_T}} \right) + \frac{1}{2} \ln m_T. \quad (12)$$

$$\frac{df}{f} = \frac{1}{2} \frac{dm}{m}. \quad (13)$$

Equation (13) gives the frequency changes that may occur due to small mass changes. The coefficient $1/2$ here is a number to be expected when the above assumptions are realized and is specific to TFs with circular cross-sections. A detailed description of this coefficient is given in Equation (14) as

$$S_{fr_circ} = \frac{\Delta f / f_0}{\Delta m / m_0} = \frac{1}{2}, \quad (14)$$

where S_{fr_circ} is defined as *fractional mass sensitivity*. In Equation (14) Δf , Δm , f_0 , and m_0 are frequency shift, etched mass, bare frequency, and bare mass respectively. The Δf is obtained by mathematically subtracting the frequency of the bare TF from the frequency of the etched TF, whereas the Δm is obtained by subtracting the mass of the bare TF from the mass of the etched TF.

Stadler et al. showed that a point mass loaded at the end of a cantilever beam has about 4 times more dominant attenuating effect on the frequency of the beam compared to a homogeneously distributed mass [68]. This result can be interpreted as follows as seen in Fig. 3. The excess mass accumulated at the ends dominates the frequency

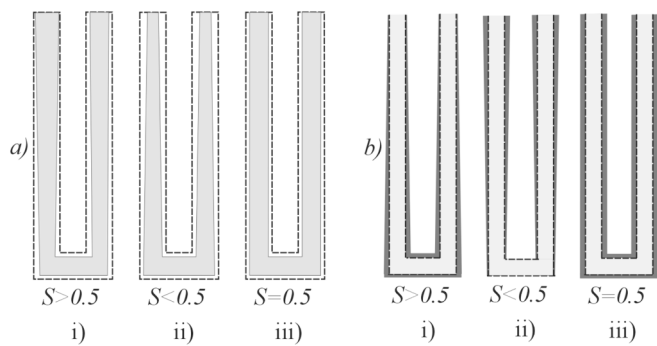


Fig. 3. Fractional mass sensitivities for a) etching and b) coating heterogeneities, respectively. a.i) little etch of the tip and much etch of the stem, a.ii) much etch of the tip and little etch of the stem, a.iii) uniform etch, b.i) little coating of the tip and much coating of the stem, b.ii) much coating of the tip and little coating of the stem, b.iii) uniform coating. The bare state before etching or coating is drawn with dashed lines, the final form with solid lines.

decreasing effect of inertia over the increasing effect of flexural rigidity and has an inversely proportional effect on the frequency. In other words, if the tip etches too much, it can be thought of as the tip disappearing. In such a case, the length is shortened, which means that the frequency will increase. Exaggerating the tip will have an inversely proportional effect on the frequency. That is, if the end regions are over-coated or etched, the frequency change shifts to the negative and the sensitivity is less than 0.5. For the opposite case, i.e. heterogeneity, where the tips are less etched, the sensitivity will be greater than 0.5.

Hypothesis: When a TF with a circular cross section is longitudinally homogeneously etched, the fractional mass sensitivity should be 0.5. In the case of longitudinal heterogeneity with more intense etching/coating at the ends, the sensitivity should be less than 0.5, and vice versa, greater than 0.5 (Fig. 3).

3. Experimental set-up and infrastructure

3.1. Material

Large-scale TFs with circular cross-sectional area and QTFs with rectangular cross-sectional area were used in this study. QTF sensors (GWX-26 series) were purchased from Gollidge Electronics Ltd. The QTFs arrived in vacuum-sealed caps outside. The cap is 2 mm wide and 6 mm long and has a frequency of 32768 Hz. The QTF frequency measurement device was produced by our department working group. This system works by stimulating the QTFs with sine signals from a DDS chip and reading the voltage values at the output (for details see Ref. [69]). Large-scale TFs made of copper and aluminum were purchased from Argeci Metal Plastik San.Tic.Ltd. Company. The copper TF has a total length of 17.3 cm and a radius of 0.15 cm. Copper II Sulfate Pentahydrate ($\text{CuSO}_4 \cdot 5\text{H}_2\text{O}$) was purchased from Beyanlab Laboratory Products San. Tic. Ltd. company. In large-scale TFs, the frequency was measured with the 'Audio Frequency Counter' programme, while the etching mass was measured with a precision balance.

3.2. Etching of large-scale tuning forks

Electrolysis, as known, is an important technique that allows mass accumulation and etching at the macro level, as seen in many products we use in our daily lives, with its parameters largely controllable. Nowadays, electrochemical machining methods are widely used in various fields such as Micro Electro Mechanical Systems (MEMS) applications [70], semiconductors [71], medicine [72], and optics [73]. For this reason, electrochemical etching method was used to etch large-scale TFs. In this study, large-scale copper tuning forks with circular cross-sections were electro-etched for different periods of time in a

saturated copper II sulfate pentahydrate ($\text{CuSO}_4 \cdot 5\text{H}_2\text{O}$) solution prepared at room temperature and a 5-volt DC power supply was used to provide the current. Copper TFs were used as anode and cathode in the electrochemical experimental setup. The etching processes were carried out in such a way that the front and then the back faces of the tuning forks were etched, respectively. During electroetching, the surface of the TF being etched may not have the same electric field strength everywhere, depending on the electrode design. In this case, more etching occurs in the areas with more electrical charge, while less etching occurs in the areas with less electrical field charge. Therefore, it is important to position the electrodes in the electrochemical experiment setup for this reason the entire surface of the anode electrode can be charged equally and thus ensure homogeneous etching. Since the equation used to calculate the frequency values is valid under the assumption of homogeneous etch, the differences in electrode designing in the electrochemical experimental setup were also evaluated (see Table 1). The appearance of the electric field lines on the TF surface when a constant voltage is applied to the metal TFs was modeled with COMSOL multiphysics 6.1. Since the electric field magnitudes measured at the end and middle points are proportional to the surface charge density, they can be used as an indicator of how intense the etching will be at that point. If the electric fields of the points are close to each other, it can be said that more longitudinal homogeneity is achieved.

TFs located at different positions will show different longitudinal etching distributions. In other words, as seen in Table 1, electric field distributions will create differences in case of etching. In this way, the effects of etching heterogeneity on fractional mass sensitivity can be monitored. Different designs have been designed for this purpose. In Design 1, the anode and cathode, which are used as TFs, are positioned parallel to each other. According to this electric field distribution, the ends of the TFs are slightly more electrically charged.

In Design 2, the anode and cathode, which are used as TFs, are positioned crosswise to each other. According to this electric field distribution, the middle parts of the TF are more electrically charged.

In Design 3, TFs used as anode and cathode are positioned in the electrochemical experimental setup with the back parts of the TFs facing each other. According to this electric field distribution, the end parts of the TF are relatively less electrically charged.

In Design 4, TFs used as anode and cathode are positioned with their ends facing each other in the electrochemical experiment setup. According to this electric field distribution, the end parts of TF are overloaded with electricity.

In Design 5 and 6, two TFs are placed parallel to the positive pole (anodes), with a parabolic copper tin in the middle connected to the negative pole (cathode). In this case, both TFs are etched. In Design 5, the copper strip, curved parabolically, serving as the cathode is positioned closer to the ends of the TF, whereas in Design 6, it is situated farther away from the ends. Consequently, in Design 5, the ends are expected to undergo more pronounced etching compared to the stem. Conversely, in Design 6, the opposite scenario is anticipated. Upon examining the electric field lines of Designs 5 and 6, it can be inferred that Design 6 will likely result in a more homogeneous etching pattern.

Table 2 shows the initial masses and frequencies and post-etch masses and frequencies of the TFs used as anodes in the six different designs mentioned above. In each experiment, two identical TFs, whose dimensions are shown in Table 2, were used as anode and cathode; therefore, the anode was abraded while the cathode was coated.

A precision balance with an accuracy of 0.01 g was used to measure the masses. To determine the etched mass, the masses of both the bare TFs and the TFs after each etching were initially measured. Subsequently, the mathematical differences between these masses were computed.

A mobile application called "Audio Spectrum Analyzer" was used for the measurement of TF vibration frequencies. After the sound frequency measurement of the application was verified with "online tone generator" programs, oscilloscope and frequency counter, the sound

Table 1
 Demonstration of electrode designs, fork formations (shapes) and electric field distributions (E. Field lines) in electrochemical experimental setup.

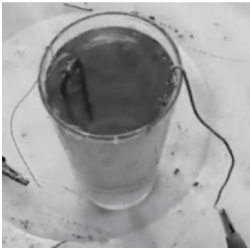
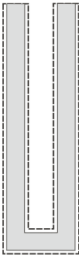
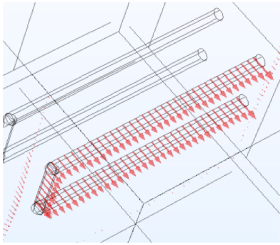

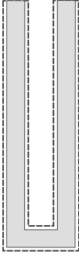
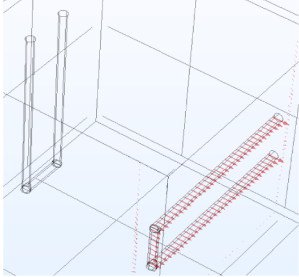

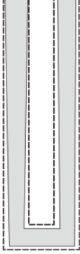
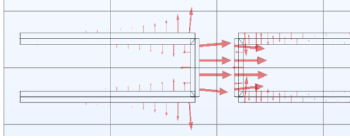
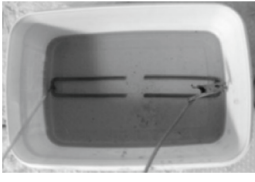
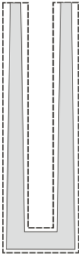
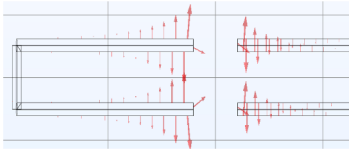
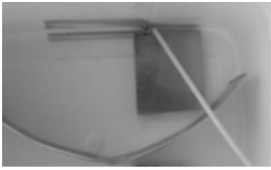
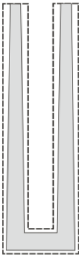
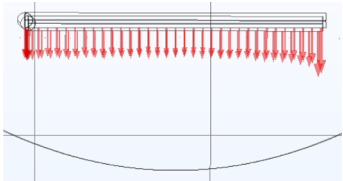
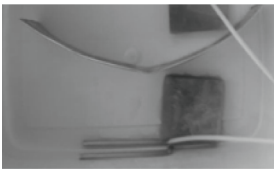
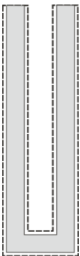
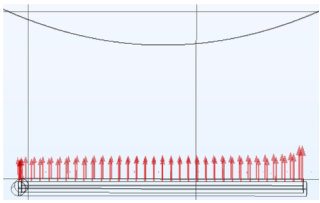
#	Photos of Electrode designs	Shapes	Drawings of electrode designs and E. Field lines
Design 1: Parallel			
Design 2: Crosswise			
Design 3: Back-to-back			
Design 4: End to end			
Design 5: Etching of two TF same time			
Design 6: Etching of two TF same time			

Table 2

Initial/final masses/frequencies, initial radius, and effective lengths of the etched TF in the designs.

	Des. 1	Des. 2	Des. 3	Des. 4	Des. 5	Des. 6
m_i (g)	9.76	6.15	10.27	9.79	7.62	7.62
m_f (g)	8.16	4.68	9.88	9.57	7.4	7.24
f_i (Hz)	254.55	628.69	254.02	237.83	411.26	419.93
f_f (Hz)	236.13	560.74	235.88	240.94	409.87	411.76
R_i (mm)	1.5	1.5	1.5	1.5	1.5	1.5
L_i (cm)	6.58	4.53	6.64	7.15	5.67	5.51

frequencies of the TFs were measured. The maximum amplitude frequency of the sound spectrum of the TF when it vibrates was considered as the fundamental mode vibration frequency. The bare frequencies measured in this way were checked and tested with the formula in Equation 7. Frequency shifts were obtained for each TF by subtracting its bare frequency from its measured frequency after each etch.

3.3. Etching of quartz tuning fork sensor surfaces

Plasma is the fourth state of matter, which is a partially ionized gas produced by providing energy to a neutral gas. Mainly produced by an electric field, plasma can also be produced by other means such as magnetic field, nuclear reaction, radio frequency, microwave, or hot filament discharge. When electrons or photons with sufficient energy collide with neutral atoms and molecules in the feed gas, electrons and ions are produced in the gas phase [21,74,75]. Plasma etching is used to remove surface material from surfaces. Surface cleaning, polishing, and roughening can be achieved by plasma etching to increase the contact area [74].

Fig. 4 shows a schematic representation of a RF generated low-pressure plasma system. The RF power source is used to generate the plasma, and the vacuum pump is used to maintain a low pressure in the plasma chamber. The plasma is generated by applying an RF voltage to two electrodes that are in the plasma chamber. The RF voltage ionizes the gas in the chamber, which creates a plasma. It is not easy to achieve nanoscale control in electrochemical etching. On the other hand, plasma etching, also known as ion milling, is a dry etching technique that allows for much more controlled and molecular-level etching, as the name implies. Therefore, in this study conducted with Quartz Tuning Forks (QTFs), plasma etching method was utilized. 4 QTF sensors with a rectangular cross-sectional area were etched separately with air plasma using a low-pressure RF plasma system. Plasma etches QTF sensors by removing material from the surface of the sensors. Placed on a glass

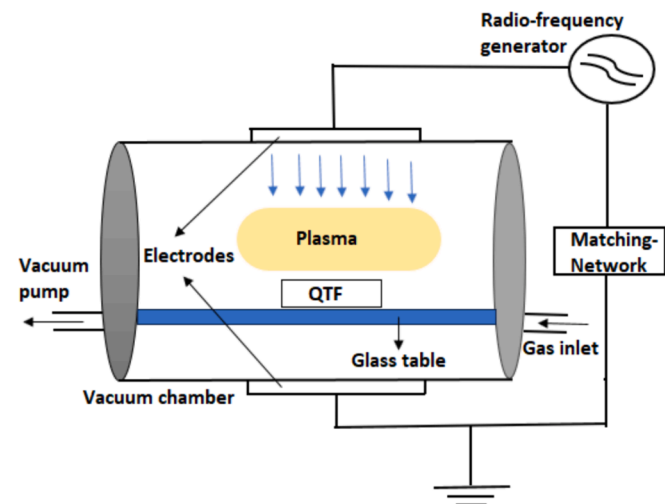


Fig. 4. Schematic representation of the radiofrequency generated low-pressure plasma system.

table, each QTF sensor was positioned in the center of the plasma chamber and the surface of the sensor was exposed to plasma radiation. In other words, 4 QTFs were etched separately under the same conditions. The etching process is controlled by plasma conditions such as power, pressure and time. The plasma conditions in this study were 20 W power, 1.5 E^{-1} torr pressure, and each etching time was 2 min.

The QTF demonstrates sensitivity at the picogram level, as evidenced in our previous study [76]. Therefore, QTFs can easily reach a point where they cannot function even with minor additions or subtractions of mass, thus exceeding the measurement range (dynamic range). Consequently, very small amounts of etching need to be conducted on the sensor surface. Based on our preliminary experiments, it was determined that exposure durations of 2 min are suitable for reasonable monitoring, and the experiments were conducted with 2-minute etching intervals. Frequency shifts were obtained for each QTF by subtracting its bare frequency from its measured frequency after each etch, and these frequencies were obtained by finding the peaks in the frequency amplitude plot [77]. These measurements were made with the frequency measuring device for which we have applied for a patent (PCT/TR2023/050453). There are two fundamental methods for measuring the frequencies of QCM and QTF. i) By constructing an oscillator suitable for the frequencies of QCM and QTF, changes in the oscillator frequency are monitored using a frequency counter. ii) When an oscillating frequency shiftable oscillator excites QCM and QTF externally, the amplitudes of the signals they pass through are summed. The frequency value with maximum amplitude corresponds to the resonance frequency of QCM or QTF. In both methods, the initial value and the frequency value after etching are noted, and the ΔF value is calculated to track mass changes. Due to the very high quality (Q) value of QTF, constructing an oscillator and reading it is relatively difficult. Therefore, in our previous studies, method "ii" has been used, as it is now much cheaper and has higher resolution. See reference [69] for more detailed information.

4. Results and discussion

4.1. Etching of large-scale tuning forks

In this section, the measured and calculated frequency shift values of large-scale copper TFs with circular cross-section after electroetching are compared. The electrodes were designed like Design 1 to each other in the experimental setup. The resonance frequencies of the large-scale TF were measured before and after each etching and calculated with Equation 7.

Fig. 5 shows the frequency shift values measured and calculated according to Equation 7 as a result of electroetching of TFs with Design 1, with the anode and cathode being copper TFs. Here, a decrease in

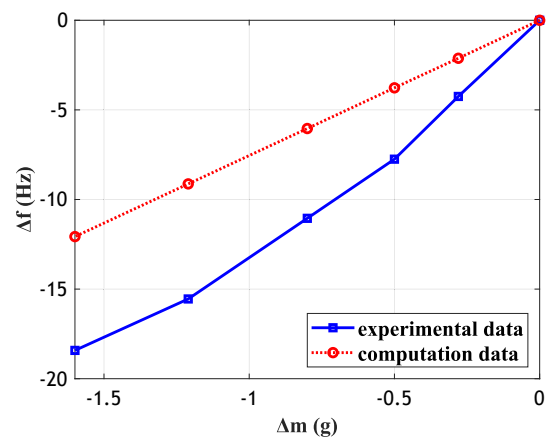


Fig. 5. Calculated and measured frequency shift values by positioning copper TFs according to Design 1.

both the measured and calculated frequency values is observed. As the etched mass increases, it is seen that the measured and calculated frequency shift values diverge. In this study, where the electrodes are designed in parallel, a visible thinning, or heterogeneity, is detected at the ends of the etched copper TFs compared to the other parts. We attribute the decrease in the agreement of the measured and calculated frequency values as the etched mass of the TFs increases to their deviation from homogeneity. In conclusion, as can be seen, the calculated and measured frequency values decreased with the etching of the surface of large-scale TFs. According to Equation 7, E (Young modulus), ρ (density of TF) remain constant during the etching of the TF, and r (radius of TF) and L (length of TF) decrease. In addition, as seen in Equation 7, it can also be said that the dominant value in the frequency drops with etching for large-scale TFs with circular cross-sections is the radius.

4.2. Etching of quartz tuning forks

QTFs were etched as described in the experimental set-up and infrastructure section.

As shown in Fig. 6, there is a decrease in frequency values with the etching of QTF sensors in bare state. According to Equation 8, which describes the frequency of QTF with rectangular cross-section used in this study, the determining dimensions are the parallel section length (b) and length (L). If the etching causes an equal decrease in all dimensions, the proportional decrease in the parallel cross-section length (b) will be more dominant than the proportional decrease in length (L), resulting in a decrease in frequency. Making surface treatments at such a thin level, i.e., at the picogram level, stable is challenging. QTF 1 and QTF 4 exhibited high compatibility. It is observed that QTF 2 and QTF 3 showed compatibility up to the 6th minute. In QCM, which is the most commonly used mass-sensitive sensor, the resonance frequencies of the sensor increase as the mass decreases from the crystal surface due to the etching of the sensor electrodes or the quartz surface in the bare state [15,52,53]. According to Equation 9 for bare QCM, h_Q is the thickness, G is the shear modulus, and ρ_Q is the density. From this equation, it can be easily derived that the frequency will increase as the thickness decreases. As in QCM, frequency increase in QTF only occurs in extreme cases, such as when the length is excessively reduced, or the thickness-length ratio is disproportionate.

4.3. Fractional mass sensitivity of tuning fork: A new approach

In this section, electro etching experiments of copper TFs used as

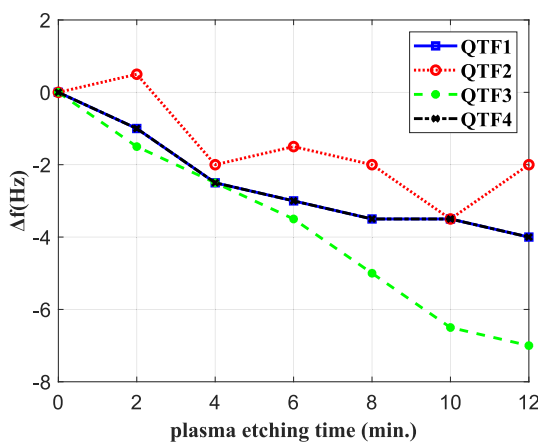


Fig. 6. By etching 4 QTF sensors under the same conditions, frequency shift values depending on the plasma etching time of each sensor (The same frequency values were seen after each etching in QTF 1 and QTF 4, so the frequency values overlapped in the graph.).

anode and cathode with various electrode designs (as shown in Table 1) were carried out and the S_{fr_circ} values obtained depending on the homogeneity of the etching were evaluated.

The electric field lines of the TFs in Design 1 can be seen in Table 1. These lines are drawn with proportional vector magnitudes and the electric field strength distribution along the TF is more uniform compared to other designs. Since the etching is directly proportional to the electric field, longitudinally homogeneous etching is assumed, and the final shape of the TF is shown in column 3. The fractional sensitivity of this design is shown in Fig. 7. In this experiment, the sensitivity of the TF at the anode was calculated as $S_{fr_circ} = 0.4752$. A total of five measurements were made and the frequency and mass measurements were plotted fractionally.

As shown in Fig. 8, TFs were placed as in Design 2 and as a result the middle parts were overcharged. Since the difference in the electric field distribution in the middle and end regions is not as high as in designs 3 and 4, it can be considered close to homogeneous. In this experiment, the sensitivity of the TF at the anode was calculated as $S_{fr_circ} = 0.4486$ and it is observed that TF frequencies decrease with etching.

Design 3 is a layout where the handle parts have excessive electric field strength. In this case the handles will be etched excessively, and the sensitivity will be greater than 0.5. In Fig. 9, the fractional mass sensitivity value is calculated as 1.8347.

Design 4 is a layout where the ends have excessive electric field strength. In this case the tips will be etched excessively, and the sensitivity will be less than 0.5. In Fig. 10, the fractional mass sensitivity value is calculated as -0.5949 . The more significant the longitudinal heterogeneity, the more the sensitivity deviates from 0.5.

The graphs of designs 5 and 6 are shown in Figs. 11 and 12 respectively. In design 5, since the edges of the parabolic cathode are close to the tip, a high electric field is generated at the ends of the TF and as a result, the tip etches more. This results in a heterogeneous shape where the tips are thinner than the center. This heterogeneous structure will reduce the sensitivity value well below 0.5. In Fig. 11, the sensitivity is calculated as 0.1223.

In design 6 the opposite is the case, and it can be predicted that the excessive thinning at the tip will be pulled to more neutral states. As a result, the sensitivity value can be estimated to be close to 0.5. In Fig. 12, the sensitivity is measured as 0.3876.

5. Conclusion and future perspective

In this work, the frequency shifts of large-scale TF and QTF surfaces due to etching were investigated mathematically and experimentally and compared with the frequency shifts caused by etching of QCM sensors. For this purpose, etching was performed on large-scale copper TFs using the electro-etching method, and on QTF sensor surfaces using the low-pressure RF plasma method. The frequency shifts were

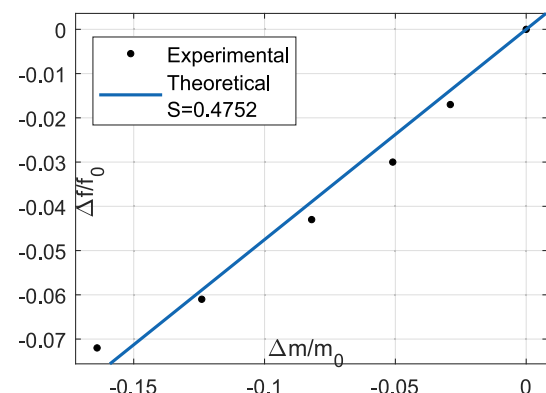


Fig. 7. Representation of the fractional mass sensitivity (S_{fr_circ}) values of the etched TF by positioning the electrodes as in Design 1.

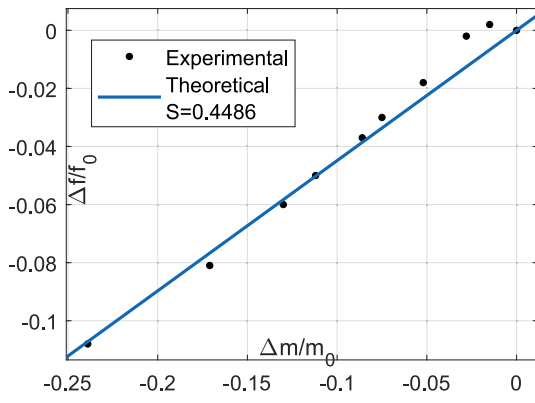


Fig. 8. Representation of the fractional mass sensitivity (S_{fr_circ}) values of the etched TF by positioning the electrodes as in Design 2.

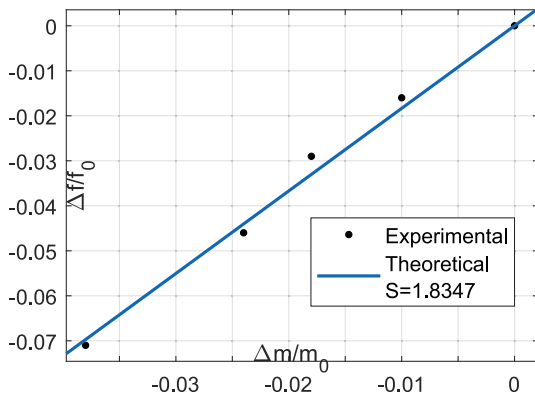


Fig. 9. Representation of the fractional mass sensitivity (S_{fr_circ}) values of the etched TF by positioning the electrodes as in Design 3.

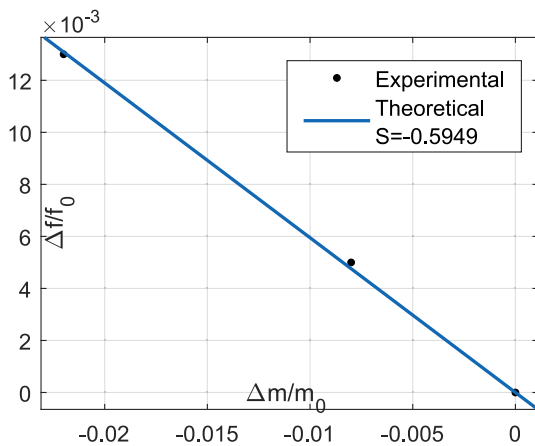


Fig. 10. Representation of the fractional mass sensitivity (S_{fr_circ}) values of the etched TF by positioning the electrodes as in Design 4.

measured and calculated. Since the equation that explains the TF resonance frequency is valid under the assumption of homogeneous etching, the etching studies of large-scale TFs were carried out in the different electrode designs (since it affects the homogeneity of the etching).

The originality of the study is based on the following two points:

- The decrease in frequency of large-scale TFs and QTF sensors etched from the bare state has been mathematically and experimentally demonstrated. The results of etching experiments with TFs and QTFs

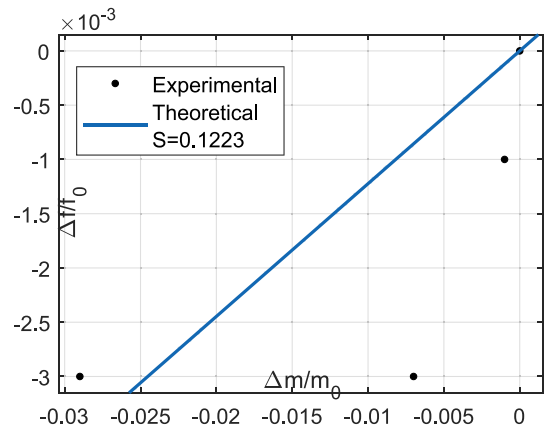


Fig. 11. Representation of the fractional mass sensitivity (S_{fr_circ}) values of the TF etched by positioning the electrodes as in Design 5.

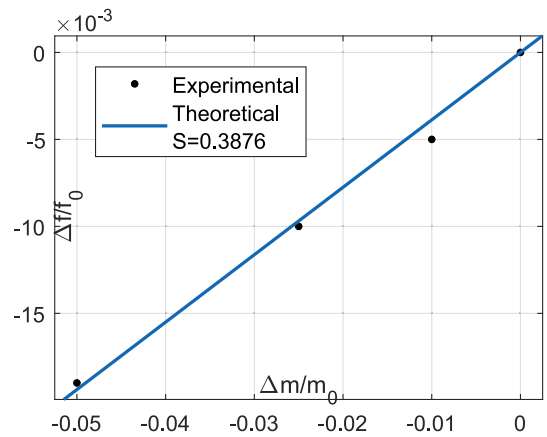


Fig. 12. Representation of the fractional mass sensitivity (S_{fr_circ}) values of the TF etched by positioning the electrodes as in Design 6.

show that as long as homogeneous etching occurs, the frequency will decrease, which is in complete contrast to QCM etching, which results in an increase in frequency.

- A new mathematical concept, fractional mass sensitivity, has been introduced to the literature. It has been mathematically and experimentally verified that the fractional mass sensitivity value defined in this study should be 0.5 under ideal conditions and with a circular cross section. To achieve fractional mass accuracy of 0.5, tuning forks must etch completely uniformly. In this context, longitudinal homogeneity holds more significance than circumferential homogeneity. These factors include longitudinal heterogeneity, circumferential heterogeneity, and roughness. However, it has been shown in this study that longitudinal heterogeneity is by far the largest source of error. If etching is performed under ideal conditions, the ratio of percent frequency shift to percent mass shift of TFs has been proven to universally yield a ratio of 0.5. With this value as a reference, very small mass shifts in QTFs can be calculated from the frequency variation.

For future studies, it is aimed to conduct more experiments on the etching of QTF sensor surfaces from the bare state and to compare them by conducting etching experiments from the bare state on QCM surfaces. Detailed studies will be conducted on the effects depending on the degree of etching. In addition, the reductions that occur in sensor surfaces due to etching should be investigated using characterization methods such as atomic force microscopy (AFM) and scanning electron microscopy (SEM).

CRediT authorship contribution statement

Kadir Can Erbaş: Writing – review & editing, Visualization, Software, Conceptualization. **Mebrure Erdoğan:** Writing – review & editing, Writing – original draft. **Dilek Çökeliler Serdaroğlu:** Writing – original draft, Supervision, Methodology. **İsmail Cengiz Koçum:** Project administration, Methodology.

Declaration of competing interest

The authors declare that they have no known competing financial interests or personal relationships that could have appeared to influence the work reported in this paper.

Data availability

Data will be made available on request.

Acknowledgments

These measurements were made with the frequency measuring device for which we have applied for a patent (PCT/TR2023/050453).

References

- Snopok, A. Laroussi, C. Cafolla, K. Voitchovsky, T. Snopok, V.M. Mirsky, Gold surface cleaning by etching polishing: optimization of polycrystalline film topography and surface functionality for biosensing, *Surf. Interfaces* 22 (July) (2020) 2021, <https://doi.org/10.1016/j.surfin.2020.100818>.
- R. Radzali, Z. Hassan, N. Zainal, F.K. Yam, Preparation of porous InAlGaN/Si(111) by photoelectrochemical etching for high performance hydrogen gas sensors at room temperature, *Sens. Actuat. B Chem.* 213 (Jul. 2015) 276–284, <https://doi.org/10.1016/j.snb.2015.02.099>.
- S. Wang, et al., Colorimetric sensor for Cr (VI) by oxidative etching of gold nanotetrapods at room temperature, *Spectrochim. Acta A Mol. Biomol. Spectrosc.* 295 (Jul. 2023), <https://doi.org/10.1016/j.saa.2023.122589>.
- M. Wu, et al., Nanogratings fabricated by wet etching assisted femtosecond laser modification of silicon for surface plasmon resonance sensing, *Appl. Surf. Sci.* 603 (2022) 154446, <https://doi.org/10.1016/j.apsusc.2022.154446>.
- X.L. Yin, et al., Multicolor enzyme-linked immunosorbent sensor for sensitive detection of organophosphorus pesticides based on TMB₂₊-mediated etching of gold nanorods, *Microchem. J.* 168 (2021) 106411, <https://doi.org/10.1016/j.microc.2021.106411>.
- W.R. Ali, M. Prasad, Fabrication of microchannel and diaphragm for a MEMS acoustic sensor using wet etching technique, *Microelectron Eng* 253(2021) (2022) 111670, doi: 10.1016/j.mee.2021.111670.
- A. A. Osipov et al., Silicon carbide dry etching technique for pressure sensors design, *J. Manuf. Process* 73(2021) (2022) 316–325, doi: 10.1016/j.jmapro.2021.11.010.
- J. Li, et al., Metal ions regulated Ag NPRs etching colorimetric sensor array for discrimination of Chinese Baijiu, *Sens. Actuat. B Chem.* 297 (June) (2019), <https://doi.org/10.1016/j.snb.2019.126715>.
- Y. Wang, M. Hu, Z. Wang, X. Liu, L. Yuan, A systematic study of the impact of etching time to the sensitivity of SiNW sensor fabricated by MACeTch process, *Mater. Sci. Semicond. Process.* 56 (May) (2016) 307–312, <https://doi.org/10.1016/j.mssp.2016.09.002>.
- S. Lee, Fabrication of an array of surface mount device 32.768 kHz quartz tuning fork-type crystals: photolithography and selective etching of an array of quartz tuning fork resonators with subsequent photoresist spray coating, *Vacuum* 65 (2) (2002) 161–168, [https://doi.org/10.1016/S0042-207X\(01\)00477-8](https://doi.org/10.1016/S0042-207X(01)00477-8).
- H. Lin, et al., Application of standard and custom quartz tuning forks for quartz-enhanced photoacoustic spectroscopy gas sensing, *Appl. Spectrosc. Rev.* 58 (8) (2023) 562–584, <https://doi.org/10.1080/05704928.2022.2070917>.
- S.H. North, E.H. Lock, C.R. Taitt, S.G. Walton, Critical aspects of biointerface design and their impact on biosensor development, *Anal. Bioanal. Chem.* 397 (3) (2010) 925–933, <https://doi.org/10.1007/s00216-010-3637-4>.
- F.A. Harraz, Porous silicon chemical sensors and biosensors: a review, *Sens. Actuat. B Chem* 202 (Oct. 2014) 897–912, <https://doi.org/10.1016/j.snb.2014.06.048>.
- D. Croux, et al., Development of multichannel quartz crystal microbalances for MIP-based biosensing, *Physica Status Solidi (A) Appl. Mater. Sci.* 209 (5) (May 2012) 892–899, <https://doi.org/10.1002/pssa.201100715>.
- T. Shiono, Y. Osada, Y. Nakagawa, Frequency change of quartz crystal resonator caused during ion beam etching, *Japanese J. Appl. Phys., Part 1: Regular Pap. Short Notes Rev. Pap.* 46(7) B (2007) 4647–4651, doi: 10.1143/JJAP.46.4647.
- C.A. Keller, B. Kasemo, Surface specific kinetics of lipid vesicle adsorption measured with a quartz crystal microbalance, *Biophys. J.* 75 (3) (1998) 1397–1402, [https://doi.org/10.1016/S0006-3495\(98\)74057-3](https://doi.org/10.1016/S0006-3495(98)74057-3).
- Y. Xianyu, Y. Lin, Q. Chen, A. Belessiotis-Richards, M.M. Stevens, M.R. Thomas, Iodide-mediated rapid and sensitive surface etching of gold nanostars for biosensing, *Angewandte Chemie - International Edition* 60 (18) (2021) 9891–9896, <https://doi.org/10.1002/anie.202017317>.
- A.M. Rossi, L. Wang, V. Reipa, T.E. Murphy, Porous silicon biosensor for detection of viruses, *Biosens. Bioelectron.* 23 (5) (2007) 741–745, <https://doi.org/10.1016/j.bios.2007.06.004>.
- A. Janshoff, H.J. Galla, C. Steinem, Piezoelectric mass-sensing devices as biosensors – an alternative to optical biosensors? *Angewandte Chemie - International Edition* 39 (22) (2000) 4004–4032, [https://doi.org/10.1002/1521-3773\(20001117\)39:22<4004::AID-ANIE4004>3.0.CO;2-2](https://doi.org/10.1002/1521-3773(20001117)39:22<4004::AID-ANIE4004>3.0.CO;2-2).
- G. Kaleli-Can, H.F. Özgüzar, M. Mutlu, Development of mass sensitive sensor platform based on plasma polymerization technique: quartz tuning fork as transducer, *Appl. Surf. Sci.* 540(2020) (2021), doi: 10.1016/j.apsusc.2020.148360.
- G. Kaleli Can, S. Mutlu, M. Mutlu, Plasma polymerized films for mass sensitive biosensors, *Nat. Appl. Sci.* 2(1) (2019) 1–7, doi: 10.38061/idunas.579225.
- C. Lou, et al., Quartz tuning fork (QTF) coating enhanced Mid-Infrared laser Induced-Thermoacoustic spectroscopy (LITES) for human exhaled methane detection, *Infrared Phys. Technol.* 133 (Sep. 2023), <https://doi.org/10.1016/j.infrared.2023.104824>.
- C. Lou, et al., Highly sensitive light-induced thermoelastic spectroscopy oxygen sensor with co-coupling photoelectric and thermoelastic effect of quartz tuning fork, *Photoacoustics* 31 (Jun. 2023), <https://doi.org/10.1016/j.pacs.2023.100515>.
- Y.H. Liu, et al., A highly sensitive LITES sensor based on a multi-pass cell with dense spot pattern and a novel quartz tuning fork with low frequency, *Opto-Electronic Adv.* 7 (3) (2024) pp, <https://doi.org/10.29026/oea.2024.230230>.
- C. Wang, et al., Miniature quartz tuning fork based light-induced thermoelastic spectroscopy sensing, *IEEE Sens. J.* (Apr. 2024), <https://doi.org/10.1109/JSEN.2024.3364095>.
- J. Dai, et al., Sensitive light-induced thermoelastic spectroscopy-based oxygen sensor with a perovskite-modified quartz tuning fork, *IEEE Sens. J.* 23 (19) (Oct. 2023) 22380–22388, <https://doi.org/10.1109/JSEN.2023.3304654>.
- X. Su, C. Dai, J. Zhang, S.J. O'shea, Quartz tuning fork biosensor, 2002. [Online]. Available: www.elsevier.com.
- A.G.T. Ruiters, J.A. Veerman, K.O. Van Der Werf, N.F. Van Hulst, Dynamic behavior of tuning fork shear-force feedback, *Appl. Phys. Lett.* 71 (1) (Jul. 1997) 28–30, <https://doi.org/10.1063/1.119482>.
- X. Zhou, T. Jiang, J. Zhang, X. Wang, Z. Zhu, Humidity sensor based on quartz tuning fork coated with sol-gel-derived nanocrystalline zinc oxide thin film, *Sens. Actuat. B Chem.* 123 (1) (Apr. 2007) 299–305, <https://doi.org/10.1016/j.snb.2006.08.034>.
- D.O. Clubb, O. V. L. Buu, R. M. Bowley, R. Nyman, J.R. Owers-Bradley, Quartz tuning fork viscometers for helium liquids, 2004.
- M. Barbic, L. Eliason, J. Ranshaw, Femto-Newton force sensitivity quartz tuning fork sensor, *Sens. Actuat. A: Phys.* 136(2) (2007) 564–566. doi: 10.1016/j.sna.2007.01.001.
- R. Blaauwgeers, et al., Quartz tuning fork: thermometer, pressure- and viscometer for helium liquids, *J. Low Temp. Phys.* 146 (5–6) (Mar. 2007) 537–562, <https://doi.org/10.1007/s10909-006-9279-4>.
- D.I. Bradley, et al., Thermometry in normal liquid ³He using a quartz tuning fork viscometer, *J. Low Temp. Phys.* 171 (5–6) (Jun. 2013) 750–756, <https://doi.org/10.1007/s10909-012-0804-3>.
- J. Zhang, S. O'Shea, Tuning forks as micromechanical mass sensitive sensors for bio- or liquid detection, *Sens. Actuat. B Chem.* 94 (1) (Aug. 2003) 65–72, [https://doi.org/10.1016/S0925-4005\(03\)00320-4](https://doi.org/10.1016/S0925-4005(03)00320-4).
- J. Zhang, C. Dai, X. Su, S.J. O'shea, Determination of liquid density with a low frequency mechanical sensor based on quartz tuning fork.
- D. Bayat, T. Akiyama, N.F. de Rooij, U. Staufer, Dynamic behavior of the tuning fork AFM probe, *Microelectron. Eng.* 85 (5–6) (2008) 1018–1021, <https://doi.org/10.1016/j.mee.2008.01.100>.
- K. Kim, J.Y. Park, K.B. Kim, N. Lee, Y. Seo, Mechanically stable tuning fork sensor with high quality factor for the atomic force microscope, *Scanning* 36 (6) (2014) 632–639, <https://doi.org/10.1002/sca.21169>.
- T. Wei et al., High and flat spectral responsivity of quartz tuning fork used as infrared photodetector in tunable diode laser spectroscopy, *Appl. Phys. Rev.* 8(4) (2021), doi: 10.1063/5.0062415.
- Y. Ma, Y. Hu, S. Qiao, Y. He, F.K. Tittel, Trace gas sensing based on multi-quartz-enhanced photoacoustic spectroscopy, *Photoacoustics* 20 (Dec. 2020), <https://doi.org/10.1016/j.pacs.2020.100206>.
- D. Zeisel, H. Menzi, L. Ullrich, A precise and robust quartz sensor based on tuning fork technology for z / SF₆-gas density control, 2000. [Online]. Available: www.elsevier.nl/locatersna.
- Q. Wang, Z. Wang, W. Ren, P. Patimisco, A. Sampaolo, V. Spagnolo, Fiber-ring laser intracavity QEPAS gas sensor using a 7.2 kHz quartz tuning fork, *Sens. Actuat. B Chem* 268 (2018) 512–518, <https://doi.org/10.1016/j.snb.2018.04.139>.
- P. Patimisco, A. Sampaolo, L. Dong, F. K. Tittel, and V. Spagnolo, “Recent advances in quartz enhanced photoacoustic sensing, *Appl. Phys. Rev.* 5(1) (2018), doi: 10.1063/1.5013612.
- S. Zhang et al., Biophotonics technologies for the detection of VOCs in healthcare applications: are we there yet? *Appl. Phys. Rev.* 10(3) (2023), doi: 10.1063/5.0145194.
- T.L.S.Q.Y.H.Z.S., Y.M. Chao Fang, Quartz-enhanced photoacoustic spectroscopy sensing using trapezoidal- and round-head quartz tuning forks, *Opt Lett* 49(3) (2024) 770–773.

- [45] K. Waszczuk et al., Evaluation of *Pseudomonas aeruginosa* biofilm formation using piezoelectric tuning forks mass sensors, *Procedia Eng.* 2010, pp. 820–823. doi: 10.1016/j.proeng.2010.09.234.
- [46] G. Gula, et al., Piezoelectric tuning fork mass sensors as a novel tool for determination of antibiotic activity on *Pseudomonas aeruginosa* biofilm, *Procedia Eng.* (2011) 980–983, <https://doi.org/10.1016/j.proeng.2011.12.241>.
- [47] T. Piasecki, G. Gula, K. Waszczuk, Z. Drulis-Kawa, T. Gotszalk, Quartz tuning fork as in-situ sensor of bacterial biofilm, in: *Procedia Engineering*, Elsevier Ltd, 2014, pp. 369–372. doi: 10.1016/j.proeng.2014.11.740.
- [48] H.F. Özgüzar, G. Kaleli Can, G. Kabay, M. Mutlu, Quartz tuning fork as a mass sensitive biosensor platform with a bi-layer film modification via plasma polymerization, *MRS Commun.* 9 (2) (2019) 710–718, <https://doi.org/10.1557/mrc.2019.55>.
- [49] D.J.D.H. Santjojo, S.P. Sakti, Masruroh, The effectivity of haloalkane (CH₂FCF₃) plasma in selective etching of a quartz crystal microbalance biosensor, in: *Proceedings - 2017 International Seminar on Sensor, Instrumentation, Measurement and Metrology: Innovation for the Advancement and Competitiveness of the Nation, ISSIMM 2017*, vol. 2017-Janua, pp. 133–136, 2017, doi: 10.1109/ISSIMM.2017.8124277.
- [50] E. Uttenhaler, M. Schräml, J. Mandel, S. Drost, Ultrasensitive quartz crystal microbalance sensors for detection of M13-Phages in liquids, *Biosens. Bioelectron.* 16 (9–12) (2001) 735–743, [https://doi.org/10.1016/S0956-5663\(01\)00220-2](https://doi.org/10.1016/S0956-5663(01)00220-2).
- [51] F. Kato, S. Nishikawa, T. Yanagida, H. Ogi, M. Hirao, Reusable high-frequency electrodeless QCM biosensor with a bare quartz resonator embedded in a silicon microchannel, in: 2011 16th International Solid-State Sensors, Actuators and Microsystems Conference, *TRANSDUCERS'11*, pp. 206–209, 2011, doi: 10.1109/TRANSDUCERS.2011.5969301.
- [52] Z. Raicheva, et al., Improving resonance characteristics of gas sensors by chemical etching of quartz plates, *J. Phys.: Conf. Series Inst. Phys. Publishing* (2012), <https://doi.org/10.1088/1742-6596/398/1/012046>.
- [53] J.L. Zhang, et al., Research on trimming frequency-increasing technology for quartz crystal resonator using laser etching, *Micromachines* (base) 12 (8) (2021) Aug, <https://doi.org/10.3390/mi12080894>.
- [54] D.E. Cliffler, A.J. Bard, Scanning electrochemical microscopy. 36. A combined scanning electrochemical microscope-quartz crystal microbalance instrument for studying thin films, 1992.
- [55] R.J. Dolleman et al., Mass measurement of graphene using quartz crystal microbalances, *Appl. Phys. Lett.* 115(5) (2019), doi: 10.1063/1.5111086.
- [56] J.H. Thomas, Etch Rates of an Electroplated Alloy (Sn-Ni) Using a Quartz Crystal Microbalance.
- [57] S. Leccia, A. Colantonio, E. Puddu, S. Galano, I. Testa, Teaching about mechanical waves and sound with a tuning fork and the Sun, *Phys. Educ.* 50 (6) (Oct. 2015) 677–689, <https://doi.org/10.1088/0031-9120/50/6/677>.
- [58] B. Kim, J. Jahng, R.M. Khan, S. Park, E.O. Potma, Eigenmodes of a quartz tuning fork and their application to photoinduced force microscopy, *Phys. Rev. B* 95(7) (2017), doi: 10.1103/PhysRevB.95.075440.
- [59] A. Kholkin, Piezoelectric materials and devices: applications in engineering and medical science, *Mater. Today* 16 (3) (Mar. 2013) 94–95, <https://doi.org/10.1016/j.mattod.2013.03.001>.
- [60] P. Patimisco, et al., Analysis of the electro-elastic properties of custom quartz tuning forks for optoacoustic gas sensing, *Sens. Actuat. B Chem.* 227 (May 2016) 539–546, <https://doi.org/10.1016/j.snb.2015.12.096>.
- [61] Y. Cheng, Z. Su, J. Zhang, Mode shape-aided cable force estimation of a double-hanger system using a vision-based monitoring method, *Measurement (Iond)* 227 (2024) 114214, <https://doi.org/10.1016/j.measurement.2024.114214>.
- [62] Y. Chen, X. An, X. Liao, Mechanical behaviors of nanowires, *Appl Phys. Rev.* 4 (3) (2017) pp, <https://doi.org/10.1063/1.4989649>.
- [63] B. Arash, J.W. Jiang, T. Rabczuk, A review on nanomechanical resonators and their applications in sensors 3 and molecular transportation, *Appl Phys. Rev.* 2 (2) (2015) pp, <https://doi.org/10.1063/1.4916728>.
- [64] L.P. Landau, L.D., E.M. Lifshitz, A.M. Kosevich, Pitaeviskii, *Theory of Elasticity*, Third. 1986.
- [65] H. Pelletier, J. Krier, A. Cornet, P. Mille, Limits of using bilinear stress-strain curve for finite element modeling of nanoindentation response on bulk materials, *Thin Solid Films* 379 (1–2) (2000) 147–155, [https://doi.org/10.1016/S0040-6090\(00\)01559-5](https://doi.org/10.1016/S0040-6090(00)01559-5).
- [66] X. Jun, Y. Bo, L. Xin, C. Juan, Theoretical model and optimization of a novel temperature sensor based on quartz tuning fork resonators, *Phys. Scr. T.* (2007) 316–320, <https://doi.org/10.1088/0031-8949/2007/T129/070>.
- [67] K. Park, M. Koh, C. Yoon, H. Kim, H. Kim, The behavior of quartz crystal microbalance in high pressure CO₂, *J. Supercrit. Fluids* 29 (1–2) (2004) 203–212, [https://doi.org/10.1016/S0896-8446\(03\)00070-6](https://doi.org/10.1016/S0896-8446(03)00070-6).
- [68] E. Macho-Stadler, M.J. Elejalde-García, R. Llanos-Vázquez, Oscillations of end loaded cantilever beams, *Eur. J. Phys.* 36 (5) (2015) 55007, <https://doi.org/10.1088/0143-0807/36/5/055007>.
- [69] M.A. Ünal, İ.C. Koçum, D. ÇökeliLer Serdaroglu, Design of a portable and low-cost mass-sensitive sensor with the capability of measurements on various frequency quartz tuning forks, *Turkish J. Electr. Eng. Comput. Sci.* 27(3) (2019) 1871–1884, doi: 10.3906/elk-1804-195.
- [70] H.C. Kim, D.H. Kim, K. Chun, Photo-assisted electrochemical etching of a nano-gap trench with high aspect ratio for MEMS applications, *J. Micromech. Microeng.* 16 (5) (May 2006) 906–913, <https://doi.org/10.1088/0960-1317/16/5/005>.
- [71] G.L. Schnable, P.F. Schmidt, Applications of electrochemistry to fabrication of semiconductor devices, *J. Electrochem. Soc.* 123 (9) (1976) 310C–C315.
- [72] M. Stöver, et al., Microstructuring of stainless steel implants by electrochemical etching, *J. Mater. Sci.* 41 (17) (Sep. 2006) 5569–5575, <https://doi.org/10.1007/s10853-006-0257-7>.
- [73] V. Torres-Costa, R.J. Martín-Palma, Application of nanostructured porous silicon in the field of optics. A review, *J. Mater. Sci.* 45 (11) (Jun. 2010) 2823–2838, <https://doi.org/10.1007/s10853-010-4251-8>.
- [74] N. Gomathi, A. Sureshkumar, S. Neogi, RF plasma-treated polymers for biomedical applications, 2008. [Online]. Available: <https://about.jstor.org/terms>.
- [75] H. Conrads, M. Schmidt, Plasma generation and plasma, *Plasma Sources Sci. Technol.* 9(4) (2000) 441–454 [Online]. Available: <https://iopscience.iop.org/article/10.1088/0963-0252/9/4/301>.
- [76] A. Dedeoglu, N. Karadas, M. Altay Unal, I. Cengiz Kocum, D. Cokeliler Serdaroglu, S. Aysil Ozkan, Calibration of quartz tuning fork transducer by coulometry for mass sensitive sensor studies, *J. Electroanal. Chem.* 834 (Feb. 2019) 8–16, <https://doi.org/10.1016/j.jelechem.2018.12.003>.
- [77] A. Alodhayb, Quartz tuning fork, a low-cost orthogonal measurement tool for the characterization of low-volume liquid reagents, *Measurement (Iond)* 152 (2020) 107313, <https://doi.org/10.1016/j.measurement.2019.107313>.